

Document downloaded from:

<http://hdl.handle.net/10251/80977>

This paper must be cited as:

Desantes Fernández, JM.; Bermúdez, V.; López, JJ.; López Pintor, D. (2016). Experimental validation of an alternative method to predict high and low-temperature ignition delays under transient thermodynamic conditions for PRF mixtures using a Rapid Compression-Expansion Machine. *Energy Conversion and Management*. 129:23-33.  
doi:10.1016/j.enconman.2016.09.089.



The final publication is available at

<http://dx.doi.org/10.1016/j.enconman.2016.09.089>

Copyright Elsevier

Additional Information

# Experimental validation of an alternative method to predict high and low-temperature ignition delays under transient thermodynamic conditions for PRF mixtures using a Rapid Compression-Expansion Machine

José M. Desantes<sup>a</sup>, Vicente Bermúdez<sup>a</sup>, J. Javier López<sup>a,\*</sup>, Darío López-Pintor<sup>a</sup>

<sup>a</sup>*CMT-Motores Térmicos  
Universitat Politècnica de València  
Camino de Vera, s/n. 46022 Valencia, SPAIN*

---

## Abstract

An alternative procedure to predict both high-temperature stage and cool flames ignition delays under transient thermodynamic conditions is intended to be validated in this paper. An experimental study has been carried out in a Rapid Compression-Expansion Machine (RCEM), using different iso-octane/n-heptane blends in order to cover a wide range of octane numbers (from 25 to 75) under a wide range of initial temperatures (from 363K to 423K), compression ratios (14 and 19), O<sub>2</sub> molar rates (from 21% to 16%) and equivalence ratios (from 0.4 to 0.8). The results obtained have been used to validate direct chemical kinetic simulations, as well as to evaluate the alternative predictive method and the Livengood & Wu integral method. Simulations have been performed solving a detailed chemical kinetic mechanism in CHEMKIN. The experimental results show good agreement with

---

\*Corresponding author  
Tel: +34 963 879 232. Fax: +34 963 877 659. E-mail: [jolosan3@mot.upv.es](mailto:jolosan3@mot.upv.es)

the chemical kinetic simulations and with the alternative predictive method. In fact, the mean relative deviation between experiments and simulations is equal to 1.7%, 2.2% and 3.1% for PRF25, PRF50 and PRF75, respectively. Besides, the alternative method has shown good predictive capability not only for the high-temperature stage of the process, but also for cool flames, being the mean relative deviation versus the experimental data lower than 3.3% for all fuels. Better predictions of the ignition delay have been obtained with the alternative procedure than the ones obtained with the classic Livengood & Wu expression, especially in those cases showing a two-stage ignition pattern, in which the Livengood & Wu integral method is not able to predict the high-temperature stage of the process.

*Keywords:* RCEM, ignition delay, autoignition modeling, fuels, chemical processes

---

## 1. Introduction, justification and objective

Regulations about pollutant emissions in internal combustion engines have become increasingly restrictive during the last years. Moreover, this trend is not only present in automotive engines, but also for naval and stationary engines. New European emission standards (Euro VI) for heavy-duty vehicles equipped with diesel engines, for instance, have reduced the  $\text{NO}_x$  limits in 80%, while the maximum soot emissions have been reduced in 50%. Since both  $\text{NO}_x$  and soot emissions cannot be simultaneously reduced in conventional diesel combustion and due to the high cost of after-treatment systems for such pollutant species, new combustion strategies have appeared as an alternative method to achieve simultaneously clean and efficient en-

12 gines.

13     Advanced combustion modes based on the autoignition of a premixed  
14 mixture with a certain degree of homogeneity have been studied for the si-  
15 multaneous reduction of soot and  $\text{NO}_x$  [1]. Their working principle is based  
16 on Low Temperature Combustion (LTC) by avoiding the soot and  $\text{NO}_x$  for-  
17 mation peninsulas, which can be seen in equivalence ratio - temperature  
18 diagrams [2], and their effectiveness has been proved in several studies [3].  
19 Despite the fact that these combustion modes show virtually zero emissions  
20 of  $\text{NO}_x$  and soot, they are characterized by high emissions of carbon monox-  
21 ide (CO) and unburned hydrocarbons (UHC), which can be easily eliminated  
22 with well-known after-treatment techniques.

23     Two main challenges appear with the implementation of these advanced  
24 combustion strategies in commercial engines: the lack of control over the  
25 autoignition process and, therefore, over the heat release rate [4]; and the  
26 operating range, which is limited to low-to-medium loads [5]. On the one  
27 hand, ignition is controlled by the chemical kinetics of the charge in these  
28 combustion modes [6]. This control entails higher complexity since there is  
29 not any explicit ignition-controlling available, such as direct injection process  
30 near top dead center or a spark. The reactivity of the mixture is modified  
31 by adjusting the engine operating conditions, including the Exhaust Gas  
32 Recirculation (EGR) rate and the inlet temperature. Therefore, improving  
33 the capability of predicting the autoignition is mandatory to properly modify  
34 the settings of the engine in order to control the heat release. On the other  
35 hand, the operating range in LTC modes is restricted to low-to-medium loads  
36 due to the fast combustion velocity of the autoignition event when the engine

37 load is increased, which results in high pressure rise rates and, therefore, in  
38 high combustion noise and mechanical strains.

39 The autoignition phenomenon can be well predicted by using advanced  
40 CFD codes with detailed chemistry and long computing times. Thus, the  
41 computational cost is too high for the implementation of such methodologies  
42 in an engine control unit, in which only simple numerical methods can be  
43 implemented. If these low computing time predictive methods have enough  
44 accuracy on the prediction of the ignition delay, the control of the engine  
45 can be significantly improved since decisions in real time can be taken. The  
46 Livengood & Wu integral method [7] allows to obtain ignition delays of pro-  
47 cesses under transient thermodynamic conditions by using the ignition times  
48 at constant temperature and pressure conditions, which can be obtained ex-  
49 perimentally and by simulation, and easily parameterized. The expression  
50 proposed by these authors is the following:

$$\int_0^{t_i} \frac{1}{\tau} dt = 1 \tag{1}$$

51 where  $t_i$  is the time of ignition of the process and  $\tau$  is the ignition delay time  
52 under constant conditions for the successive thermodynamic states.

53 The Livengood & Wu integral defined the ignition event as the instant  
54 at which a critical concentration of chain carriers is reached, assuming that  
55 the critical concentration is constant whatever the thermodynamic condi-  
56 tions for a certain air-fuel mixture. Besides, the integral method describes  
57 the decomposition of the fuel during the ignition delay by a single zero-order  
58 global reaction that cannot properly model the negative temperature coef-  
59 ficient (NTC) behavior. This predictive method has been enunciated as a

60 characterization of knock in SI-engines [8]. However, nowadays it has become  
61 more relevant for CI-engines, in which it can be used as a method for the  
62 prediction of the ignition characteristics of homogeneous mixtures as the ones  
63 used in LTC combustion modes [9]. Several authors such as Ohyama [10],  
64 Rausen et al. [11], Choi et al. [12] and Hillion et al. [13] studied the im-  
65 plementation of the Livengood & Wu integral method in an engine control  
66 unit. The integral method has been used to predict the ignition event under  
67 HCCI conditions, so that it can be combined with some other simple models  
68 to characterize the combustion process, allowing the control of the engine in  
69 real time.

70 Since the Livengood & Wu integral method is based on a single global  
71 reaction mechanism that ignores the cool flames and the NTC behavior, it  
72 seems to not be able to accurately predict the ignition delay when a two-  
73 stage ignition occurs, as it has been wondered by several authors [14]. Some  
74 of these authors, as Liang and Reitz [15] or Edenhofer et al. [16], show  
75 the need to propose simple numerical methods to predict the ignition time  
76 in a simple way and with low computational cost, but avoiding the most  
77 restrictive hypotheses of the integral method, in order to be able to characterize  
78 the low-temperature autoignition phenomenon avoiding any chemical kinetic  
79 mechanism. However, few alternative predictive methods can be found in  
80 the literature.

81 Hernandez et al. [17] studied the accuracy of the Livengood & Wu integral  
82 by solving different chemical kinetic mechanisms for different fuels by sim-  
83 ulation in CHEMKIN. They checked that, if the fuel follows a single-stage  
84 ignition pattern, quite good prediction capability is shown by the integral

85 method. Two alternative procedures have been proposed by these authors,  
86 resulting one of them in better results than the Livengood & Wu integral.  
87 However, the same hypotheses than the integral method are assumed in most  
88 of the alternative procedures proposed, since they are based on the Livengood  
89 & Wu integral itself.

90 Desantes et al. [18, 19] have proposed different methods based on the  
91 Glassman's model to predict ignition delays referred to a critical concentra-  
92 tion of chain carriers. The hypothesis of constant critical concentration is  
93 avoided in both methods, whereas one of them also avoids the description  
94 of the autoignition process by a single zero-order global reaction. However,  
95 since the ignition delay is defined as the time when a critical concentration of  
96 chain carriers is reached, only ignition delays referred to critical concentra-  
97 tions can be predicted accurately. Therefore, the high exothermic phase of  
98 the ignition cannot be obtained, since the critical concentration occurs in a  
99 previous stage. Desantes et al. [20] have also proposed an alternative method  
100 to predict both high-temperature stage and cool flames ignition delays under  
101 transient thermodynamic conditions, which is a previous work related to the  
102 current one. This alternative method has been validated for pure n-heptane  
103 and pure iso-octane. However, both fuels define the extreme values of the  
104 octane number reference scale and a wider validation among all the octane  
105 number scale is needed for a better evaluation of the predictive method.

106 Dual-fuel combustion based on diesel/gasoline mixtures has shown to be  
107 a good method to increase the operating range of LTC modes. Bessonette  
108 et al. [21] have shown that different in-cylinder reactivities are required for  
109 a proper LTC operation under different working conditions. Specifically, low

110 octane fuels are required at low loads, while high octane fuels are needed at  
111 medium-to-high loads. A wide range of octane numbers can be achieved by  
112 using premixed gasoline mixtures in which a direct diesel injection causes an  
113 stratification of reactivities [1]. Thus, a flexible operation over a wide operat-  
114 ing range is possible by modifying both the blending ratio between fuels and  
115 the direct injection settings. Therefore, predictive methods to improve the  
116 engine control should be validated not only for diesel and gasoline surrogate  
117 fuels, but also for a wide range of reactivities (i.e. of octane numbers).

118 The validity of an alternative procedure to determine both high-temperature  
119 and cool flames ignition delays under transient conditions is intended to be  
120 solved in this work for a wide range of octane numbers. The study has been  
121 done with different n-heptane and iso-octane blends, the reactivities of which  
122 are very similar to diesel fuel and gasoline, respectively. These Primary Ref-  
123 erence Fuels blends (PRFs) are used to define the octane number reference  
124 scale. More specifically, PRF25 (25% iso-octane), PRF50 (50% iso-octane)  
125 and PRF75 (75% iso-octane) have been evaluated in this work, which octane  
126 numbers are equal to 25, 50 and 75, respectively. Besides, PRFs mixtures  
127 were chosen because extended and fully validated chemical kinetic mecha-  
128 nisms are available for them.

129 Simulations have been performed with the software of chemical simulation  
130 CHEMKIN (Reaction Design, ANSYS), which is consolidated in engineering  
131 investigations, so that the oxidation paths of several hydrocarbons are de-  
132 scribed by chemical kinetics mechanisms ready to be used with it. Finally, the  
133 numerical results are validated experimentally using a Rapid Compression-  
134 Expansion Machine (RCEM).



135 The structure of the paper is the following: first, the experimental fa-  
136 cility (RCEM) that has been used in this work is described. Then, the  
137 methodological approach is presented, including the experimental methods,  
138 the alternative predictive procedure, the chemical kinetic simulations and  
139 the parametric study performed. Afterwards, the experimental ignition de-  
140 lays are analyzed, the predictive method is validated with the experimental  
141 results and its predictive ability is compared with the chemical kinetic sim-  
142 ulations and with other methods. Finally, the conclusions of this study are  
143 shown.

## 144 **2. Materials and methods**

145 An alternative method to predict ignition delays proposed by Desantes  
146 et al. [20] was tested by comparison with the experimental results from a  
147 RCEM. For a certain case, the in-cylinder temperature and pressure were  
148 experimentally obtained under motoring conditions (without combustion).  
149 Then, the ignition characteristics for each thermodynamic state (ignition de-  
150 lay,  $\tau$ , and critical concentration,  $[CC]_{max}$ ) were obtained by simulation in  
151 CHEMKIN solving a detailed mechanism in a perfectly stirred reactor. The  
152 ignition delay under transient thermodynamic conditions was measured di-  
153 rectly from the experiments in the RCEM. Besides, it was also simulated  
154 in CHEMKIN solving the same detailed mechanism in an internal combus-  
155 tion engine reactor (direct chemical simulation). This ignition time is finally  
156 predicted by using the alternative procedure analyzed in this paper and the  
157 Livengood & Wu integral method. Finally, the simulated and predicted ig-  
158 nition delays were compared with the experimental measurements.

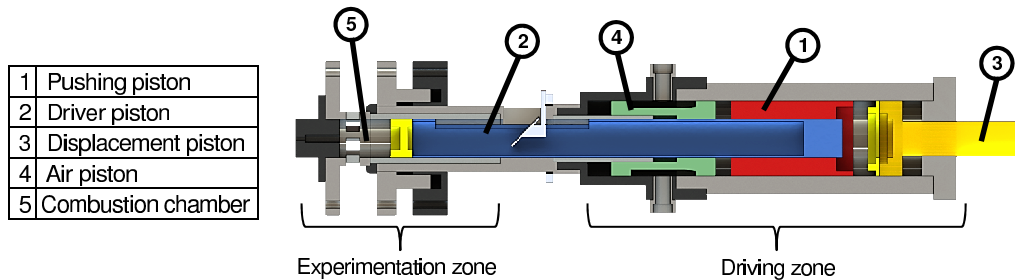


Figure 1: Rapid Compression Expansion Machine schematic.

159 *2.1. RCEM*

160 An RCEM is an useful experimental facility widely used in combustion  
 161 studies due to its capability to replicate engine conditions under fully con-  
 162 trolled initial and boundary conditions [22]. Not only the in-cylinder engine  
 163 thermodynamic conditios can be replicated, but also the combustion phe-  
 164 nomenon, while avoiding the complexities associated to engines [23].

165 Stroke and clearance volume can be modified in order to reproduce differ-  
 166 ent engine geometrical characteristics, resulting in the capability of working  
 167 with a wide range of compression ratios. Besides, the engine speed can be  
 168 simulated by changing the compression velocity. A full diagnosis of the com-  
 169 bustion process under engine conditions can be carried out, since not only  
 170 the compression, but also the expansion stroke is replicated. Despite the fact  
 171 that homogeneous mixtures are usually tested in autoignition studies to be  
 172 able to trace the chemical kinetics in a easier way, heterogeneous mixtures  
 173 can be also studied in this facility by injecting the fuel during the compres-  
 174 sion stroke, as well as new combustion modes such as the dual fuel technology  
 175 [24] or LTC modes [25].

176 Figure 1 shows a schematic of the RCEM, in which two different zones can  
 177 be distinguish: an experimentation zone and a driving zone. Four pistons  
 178 compose the driving section. The pushing piston is pneumatically driven  
 179 by the compressed air contained in the air piston and hydraulically coupled  
 180 to the driver piston, which compresses the test sample into the combustion  
 181 chamber. The stroke is selected by changing the position of the displacement  
 182 piston, which is hydraulically driven. A wide explanation about the operation  
 183 principle of the RCEM can be read in [19].

Bore	84	mm
Stroke	120 - 249	mm
Compression ratio	5 - 30	-
Maximum cylinder pressure	200	bar
Initial pressure	1 - 5	bar
Maximum heating temperature	473	K

Table 1: Technical characteristics of the RCEM.

184 Table 1 shows the range of operating conditions that can be performed  
 185 in the RCEM. The positions of both, the pushing piston and the driver  
 186 piston, are measured by two AMO LMK102 incremental position sensors  
 187 with  $0.01\text{ mm}$  of resolution. This way, the piston position and, consequently,  
 188 the combustion chamber volume are known. The experimentation piston  
 189 that compresses the test sample into the combustion chamber is composed  
 190 by the head of the driver piston, which is  $84\text{ mm}$  in bore and includes a  
 191 cylindrical bowl,  $46\text{ mm}$  in bore and  $17\text{ mm}$  in depth.

192 The initial temperature, as well as the temperature of the walls, are con-

193 trolled by a PID regulator that acts over an electrical 80  $W$  heater located  
194 in the bowl and two more spire-shape electrical heaters (600  $W$  each) lo-  
195 cated in the liner. the control loop is possible by measuring the temperature  
196 by three thermocouples located in the liner, in the piston and in the bowl,  
197 respectively. The intake and exhaust pipes, which are located in the liner,  
198 are designed to induce a swirl motion into the combustion chamber during  
199 the intake process. A homogeneous environment is guaranteed by the high  
200 level of turbulence generated during the filling, being the initial temperature  
201 equal to the wall temperature (checked by previous CFD studies). A Kistler  
202 6045A uncooled piezoelectric pressure sensor located in the cylinder head  
203 (-45  $pC/bar$  of sensitivity) is coupled to a Kistler 5018 charge amplifier for  
204 the measurement of the in-cylinder pressure. Besides, the filling of both, the  
205 combustion chamber and the driving gas volume are controlled by three Wika  
206 piezoresistive pressure sensors (0.01  $bar$  of resolution). Finally, a common  
207 rail system that includes a 7-hole nozzle implemented in a BOSCH solenoid-  
208 commanded injector that is controlled by a EFS IPod power driving module  
209 forms the injection system, which has been characterized as explained in [26].

210 A Yokogawa DL850V system composed by one 10  $MHz$ -12 bits module  
211 and five more 1  $MHz$ -16 bits modules with two channels each acts as acqui-  
212 sition system, in which 10  $MHz$  are fixed as acquisition frequency. Such a  
213 high acquisition frequency is mandatory to be able to measure the electrical  
214 pulses of the incremental position sensor. However, both, in-cylinder and  
215 injection pressures are recorded at 1  $MHz$ .

216 A heated external tank (up to 5204  $K$  by three electrical heaters, 1200  $W$   
217 each) is used for the generation of the synthetic air, which is produced by

218 mixing  $N_2$ ,  $CO_2$  and  $O_2$  according to their partial pressures. Moreover,  $H_2O$   
219 can be added thanks to a syringe pump. Vacuum is created before generating  
220 each mixture and before filling the RCEM to ensure the no contamination  
221 in this tank, nor in the combustion chamber. Finally, the exact composition  
222 of the synthetic mixture is measured by gas chromatography in a Rapid  
223 Refinery Gas Analyser from Bruker (450-GC) in order to ensure the correct  
224 reproduction of the experiments in CHEMKIN.

225 Figure 2 shows the move law of the RCEM compared to an engine. It  
226 can be seen that both paths are really similar around TDC. Besides, the  
227 pressure signal under motoring conditions is also plotted in the figure. The  
228 time reference ( $t = 0$ ) is taking as the instant at which the piston position  
229 reaches 29 *mm*, since it coincides with the start of the rapid compression  
230 stroke because of constructive aspects of the RCEM [19].

231 In this study, the synthetic EGR was considered to be composed by the  
232 products of a dry air/fuel complete combustion reaction in which the oxygen  
233 content is the one selected by the user, as explained in [27]. In order to avoid  
234 stratification problems, the fuel is injected into the combustion chamber at  
235 the beginning of the intake process, in which the turbulence generated, as  
236 well as the duration time ( $\approx 40$  s), are enough to guarantee a homogeneous  
237 environment when the compression stroke starts.

238 The ignition of the mixture is defined as the maximum time derivative of  
239 the pressure signal (pressure rise rate), so that the experimental ignition de-  
240 lay is defined as the time between the start of the rapid compression process,  
241 which is unambiguously defined because of constructive aspects of the ma-  
242 chine, and the instant in which the maximum pressure rise is measured. An

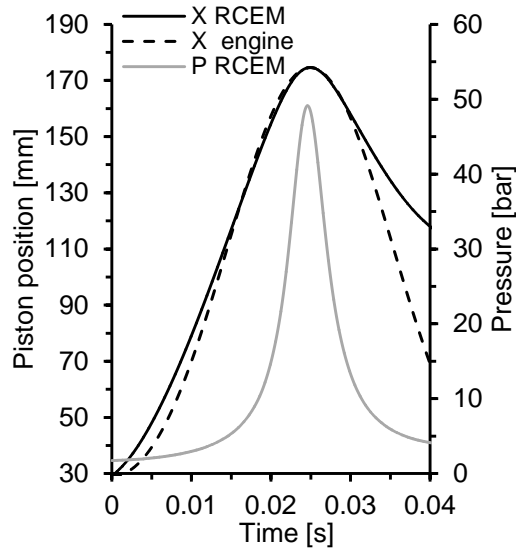


Figure 2: Move law of the RCEM compared to an engine and pressure path under motoring conditions.

243 example of the ignition delay definition can be seen in Fig. 3, in which cool  
 244 flames and the high temperature ignition delay can be distinguished when  
 245 a two-stage ignition pattern occurs. Furthermore, the number of repetitions  
 246 for each operating condition has been selected so that the semi-amplitude of  
 247 the confidence interval with a level of confidence of 95% is smaller than 1%  
 248 of the mean ignition delay value. Thus, a representative ignition delay time  
 249 measurement is ensured.

250 Finally, the temperature profile is calculated by solving the equation of  
 251 state, in which the in-cylinder pressure and the piston position are measured.  
 252 Furthermore, a model for deformations and another one for leaks (explained  
 253 in [28, 29]) are taken into account. The heat losses, which are needed to  
 254 replicate the experiments in CHEMKIN, are characterized by a model based

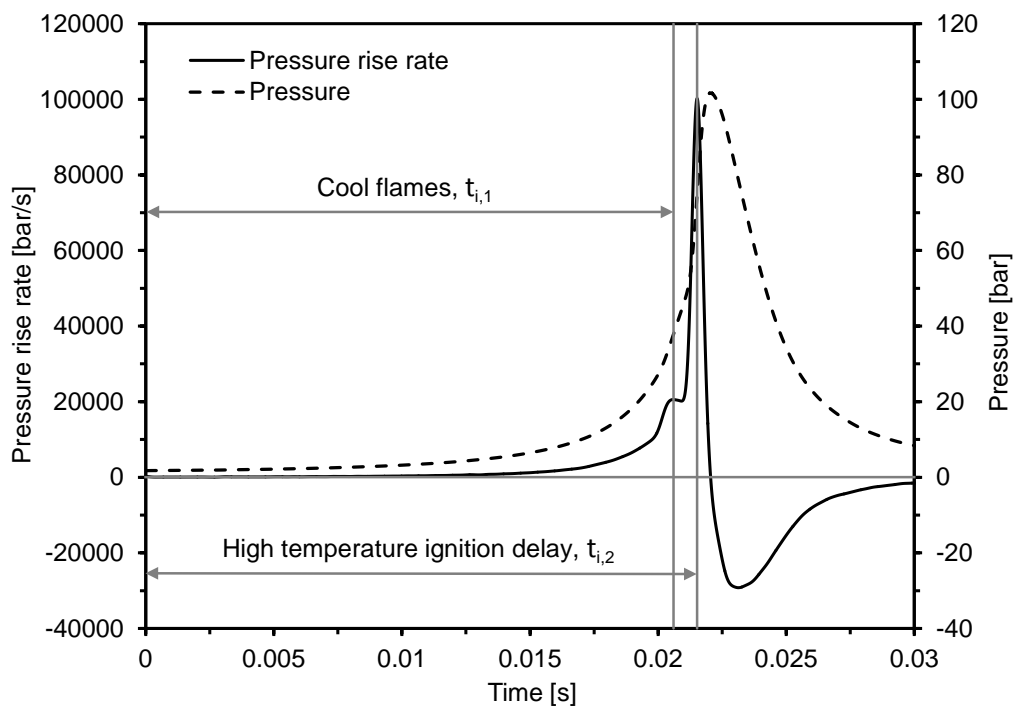


Figure 3: Ignition delay definition. The autoignition of the mixture is considered to be produced when the maximum pressure rise occurs.

255 on the Woschni correlation [30].

## 256 2.2. Alternative predictive method for ignition delays

257 The predictive procedure proposed by Desantes et al. [20] is composed  
258 by two different consecutive integrals:

$$1 = \frac{1}{[CC]_{max,t_{i,CC}}} \int_0^{t_{i,CC}} \frac{[CC]_{max}}{\tau_{CC}} dt \quad (2)$$

$$1 = \frac{1}{[CC]_{max,t_{i,CC}}} \int_{t_{i,CC}}^{t_{i,2}} \frac{[CC]_{max}}{\tau_2 - \tau_{CC}} dt \quad (3)$$

259 where  $t_{i,CC}$  is the ignition delay of the process referred to a maximum con-  
260 centration of chain carriers and  $t_{i,2}$  is the ignition delay referred to the high-  
261 temperature stage of combustion. Besides,  $\tau_2$ ,  $\tau_{CC}$  and  $[CC]_{max}$  are the  
262 ignition delay referred to the high exothermic stage, the ignition delay re-  
263 ferred to a maximum of chain carriers and the critical concentration of chain  
264 carriers, respectively, under constant conditions of pressure and temperature  
265 for the successive thermodynamic states.

266 The method is decoupled in two steps depending on the stage of the igni-  
267 tion to predict. On the one hand, a predictive method for cool flames is based  
268 on the accumulation of chain carriers up to reach the critical concentration.  
269  $\text{HO}_2$  is selected as chain carrier since it seems to be a good tracer of such  
270 phenomenon ( $CC=\text{HO}_2$ ). The accumulation of  $\text{HO}_2$  is modeled by Eq. 2, in  
271 which  $\tau_{CC}$  and  $[CC]_{max}$  are related with this species. The upper limit of the  
272 integral represents the instant at which the maximum concentration of  $\text{HO}_2$   
273 occurs, which corresponds to the ignition delay referred to cool flames.

274 On the other hand, a predictive method for the high-temperature stage  
275 of the combustion process is based on the accumulation of chain carriers up



276 to the critical concentration (Eq. 2), and the subsequent consumption from  
277 this maximum of concentration (Eq. 3). Thus, two different consecutive  
278 integrals have to be solved in this method.  $\text{CH}_2\text{O}$  is selected as chain carrier  
279 ( $\text{CC}=\text{CH}_2\text{O}$ ), since formaldehyde is widely recognized as an autoignition  
280 tracer and the maximum heat release rate occurs when this species is almost  
281 consumed [31]. The instant at which the maximum concentration of  $\text{CH}_2\text{O}$   
282 is reached is obtained by solving Eq. 2, whereas the consumption of  $\text{CH}_2\text{O}$   
283 is modeled by Eq. 3. Obviously,  $\tau_{\text{CC}}$  and  $[\text{CC}]_{\text{max}}$  have to be related with  
284 this species. The upper limit of the integral in Eq. 3 represents the time at  
285 which all formaldehyde is consumed, which corresponds to the ignition delay  
286 referred to the high-temperature stage.

287 A detailed description about the theoretical development that defines the  
288 method can be found in [19, 20].

### 289 *2.3. CHEMKIN and chemical kinetic mechanisms*

290 CHEMKIN-PRO is the software used to obtain the different ignition de-  
291 lays and critical concentrations. The Curran’s kinetic mechanism, which  
292 is composed by 1034 species and 4238 reactions, is used for n-heptane/iso-  
293 octane blends [32, 33]. This mechanism includes the chemical kinetics of the  
294 two pure hydrocarbons that form the blends used in this investigation, the  
295 validity of which has been checked in different papers by comparison with  
296 experimental results [34, 35].

297 Different ignition delays are defined in the simulations:

- 298 •  $\tau_1$  is the ignition delay under constant thermodynamic conditions re-  
299 ferred to the maximum pressure rise caused by cool flames.

- 300 •  $\tau_2$  is the ignition delay under constant thermodynamic conditions re-  
301 ferred to the maximum pressure rise caused by the high-temperature  
302 stage of the combustion process.
- 303 •  $\tau_{CC}$  is the ignition delay under constant thermodynamic conditions  
304 referred to the critical concentration of chain carriers. Different species  
305 are proposed as chain carrier depending on the stage of the ignition to  
306 be predicted:  $CC=HO_2$  for cool flames and  $CC=CH_2O$  for the high-  
307 temperature stage of the process.
- 308 •  $t_{i,1}$  is the ignition delay under transient thermodynamic conditions re-  
309 ferred to the maximum pressure rise caused by cool flames. This igni-  
310 tion delay is also experimentally obtained.
- 311 •  $t_{i,2}$  is the ignition delay under transient thermodynamic conditions re-  
312 ferred to the maximum pressure rise caused by the high-temperature  
313 stage of the combustion process. This ignition delay is also experimen-  
314 tally obtained.

315 The model used for the calculation of ignition delays under constant con-  
316 ditions ( $\tau_1$ ,  $\tau_2$  and  $\tau_{CC}$ ) and critical concentrations is a perfectly stirred reac-  
317 tor (PSR), which is a homogeneous closed reactor that works under constant  
318 pressure and uses the energy equation to obtain the temperature evolution.  
319 As it has been demonstrated by Payri et al. [36], this model is the most  
320 suitable to simulate ignition delays at constant thermodynamic conditions.

321 The model used for the calculation ignition delays under transient con-  
322 ditions ( $t_{i,1}$  and  $t_{i,2}$ ) is a reciprocating internal combustion engine that op-  
323 erates under homogeneous conditions (IC-engine, closed 0-D reactors from

324 CHEMKIN). Both, heat losses and the volume profile are imposed in order to  
325 reproduce the experimental conditions reached in the combustion chamber of  
326 the RCEM. The piston starts at bottom dead center (BDC) and a complete  
327 cycle is simulated, i.e., compression and expansion strokes. The autoignition  
328 is considered to be produced when the pressure rise rate reaches a maximum,  
329 which is the same criterion than the one used in the experiments. Therefore,  
330 the simulated results can be directly compared with the experimental ones.

331 Finally, the ignition delays and the critical concentrations are obtained  
332 for each thermodynamic state of the transient process with a  $\Delta t$  of  $10^{-5}s$ ,  
333 which is a compromise value between prediction accuracy and computing  
334 time. Moreover, 30 s have been selected as the maximum waiting time for  
335 the autoignition of the mixture under constant conditions.

#### 336 2.4. Parametric study performed

337 The performed experimental study was as follows:

- 338 • Fuel: PRF25, PRF50 and PRF75.
- 339 • Initial temperature ( $T_i$ ): 363 K, 383 K, 403 K and 423 K.
- 340 • Initial pressure ( $P_i$ ): 0.15 MPa.
- 341 • Compression stroke: 180 mm.
- 342 • Compression ratio ( $CR$ ): 14 and 19.
- 343 • Oxygen molar fraction ( $X_{O_2}$ ): 0.21, 0.18 and 0.16.
- 344 • Equivalence ratio ( $Fr$ ): from 0.4 to 0.8 depending on the fuel and on  
345 the oxygen molar fraction.

346 The performed parametric study can be seen in Table 2. The oxygen  
 347 molar fraction limits the maximum working equivalence ratio in order to  
 348 avoid extremely violent combustions that can damage the facility. It should  
 349 be noted that the initial temperature is higher than the boiling point of the  
 350 fuel, ensuring that the fuel is always in vapor phase before the beginning of  
 351 the cycle.

		$X_{O_2}$		
		<b>0.21</b>	<b>0.18</b>	<b>0.16</b>
$T_i$	<b>363</b>	0.4, 0.5, 0.6	<i>0.4</i> , 0.5, 0.6, <b>0.7</b>	
	<b>383</b>	0.4, 0.5, 0.6	<i>0.4</i> , 0.5, 0.6, <b>0.7</b>	0.5, 0.6, 0.7, <u>0.8</u>
	<b>403</b>	0.4, 0.5, 0.6	<i>0.4</i> , 0.5, 0.6, <b>0.7</b>	
	<b>423</b>	0.4, 0.5, 0.6	<i>0.4</i> , 0.5, 0.6, <b>0.7</b>	0.5, 0.6, 0.7, <u>0.8</u>

Table 2: Parametric study performed. Equivalence ratio for different initial temperatures and oxygen molar fractions. *Italic.*- exclusively for CR 19. **Bold.**- exclusively for CR 14. Underlined.- exclusively for PRF75.

### 352 3. Results and validation

353 The experimental trends of the ignition delay are discussed in this section.  
 354 Besides, ignition delays calculated by solving the detailed chemical kinetic  
 355 mechanism for n-heptane/iso-octane blends are compared with the experi-  
 356 mental results in order to validate the mechanism in the working range. The  
 357 experimental ignition delay predicted by means of two different methods:  
 358 using the alternative integral method proposed by Desantes et al. [20] and  
 359 using the Livengood & Wu integral method. The two different exothermic

360 stages of the auto-ignition process have been studied: cool flames and the  
361 high-temperature stage of the process.

### 362 *3.1. Experimental trends of the ignition delay*

363 Figs. 4, 5 and 6 show the ignition delay trends versus temperature for  
364 PRF25, PRF50 and PRF75, respectively, under different compression ratios  
365 and oxygen molar fractions. It can be seen that the ignition delay decreases if  
366 the temperature is increased except in the Negative Temperature Coefficient  
367 (NTC) zone [37]. Despite the fact that the NTC behavior can be smooth  
368 enough to avoid an increase of the ignition delay (such as under  $Fr = 0.6$ ,  $CR$   
369  $= 19$ ,  $X_{O_2} = 0.21$  for the three fuels), the ignition delay decreasing rate is  
370 usually affected by this phenomenon, changing the slope of the curve. Higher  
371 temperatures imply higher collision frequencies and collision energies and,  
372 therefore, higher specific accumulation rates of chain carriers and shorter  
373 ignition delays. During the NTC zone, the accumulation of chain carriers  
374 competes with the formation of stable long-chain olefins by the alkyl radicals,  
375 which causes a decrease of reactivity that results in longer ignition delays.

376 The dependence of the ignition delay on the compression ratio can be  
377 also seen in Figs. 4, 5 and 6 for PRF25, PRF50 and PRF75, respectively.  
378 The ignition delay decreases when the compression ratio is increased, since  
379 higher pressures and temperatures are reached. Moreover, Fig. 4 shows that,  
380 in general, the NTC zone becomes less pronounced if the pressure is increased.  
381 The end of the NTC zone is controlled by the unimolecular fall-off reaction  
382  $H_2O_2 + M = OH + OH + M$ , which is a third body reaction the specific  
383 reaction rate of which increases if the pressure is increased.

384 The effects of the equivalence ratio on the ignition delay under low tem-

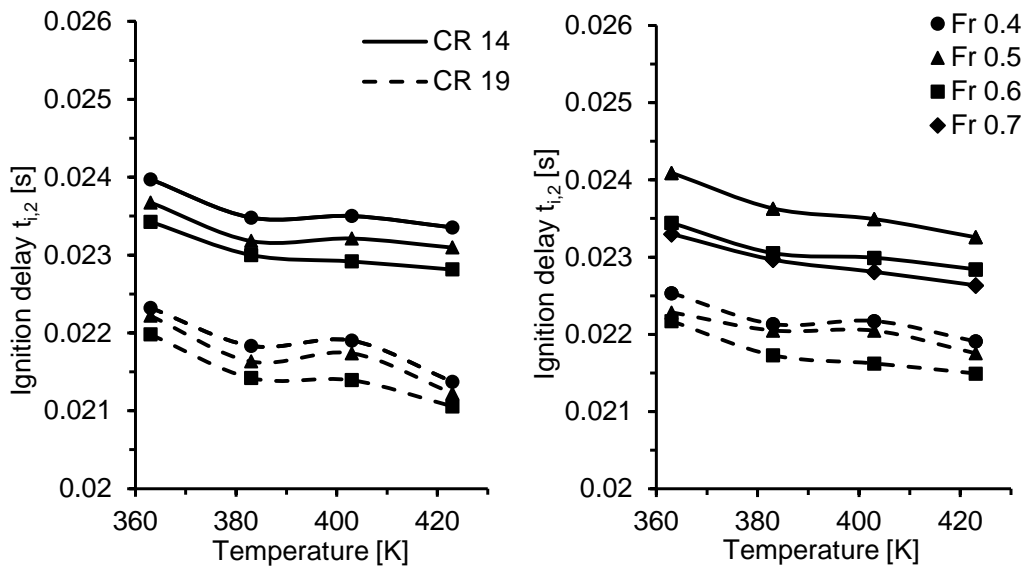


Figure 4: Ignition delay,  $t_{i,2}$ , versus initial temperature for PRF25. Both compression ratios are plotted. Left.-  $X_{O_2} = 0.21$ . Right.-  $X_{O_2} = 0.18$ .

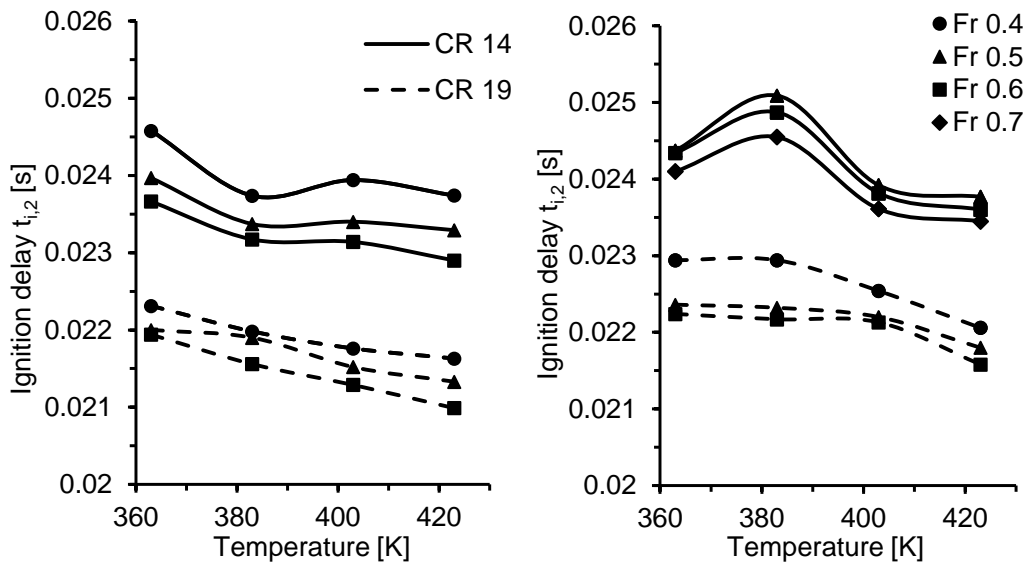


Figure 5: Ignition delay,  $t_{i,2}$ , versus initial temperature for PRF50. Both compression ratios are plotted. Left.-  $X_{O_2} = 0.21$ . Right.-  $X_{O_2} = 0.18$ .

385 perature conditions are also plotted in Figs. 4, 5 and 6 for PRF25, PRF50  
386 and PRF75, respectively. The ignition delay referred to the high-exothermic  
387 stage of the process decrease when the equivalence ratio is increased, since  
388 ignition is triggered when a critical concentration of chain carriers is reached.  
389 The accumulation of chain carriers depends on the amount of fuel, so that the  
390 higher the equivalence ratio, the higher the generation rate of chain carriers  
391 and the shorter the ignition delay. Moreover, the lower the compression ratio  
392 or the lower the amount of oxygen, the higher the effect of the equivalence  
393 ratio on the ignition delay. I.e., the ignition delay is more sensitive to changes  
394 in the equivalence ratio if the reactivity of the mixture is reduced, since the  
395 low-temperature chain branching reactions, which depend on the amount of  
396 fuel, are more dominant. Besides, it can be seen in the figures that the NTC  
397 zone becomes less pronounced if the equivalence ratio is increased.

398 Fig. 7 shows the dependence of the ignition delay on the oxygen concen-  
399 tration. Ignition delay increases when the molar fraction of oxygen of the  
400 mixture is reduced, since lower amount of oxidizer implies lower reactivity.  
401 Moreover, the effect of the oxygen molar fraction becomes stronger if the  
402 equivalence ratio or the compression ratio are decreased. I.e. the ignition  
403 delay is more sensitive to changes in the oxygen content if the reactivity of  
404 the mixture is reduced, since the low-temperature chain branching reactions,  
405 which include the  $O_2$  addition, are more dominant. In the same way, it can  
406 be clearly seen in Fig. 5 that the NTC zone is moved to lower temperatures  
407 and it becomes more pronounced if the oxygen content is reduced.

408 Finally, the effects of the octane number on the ignition delay can be seen  
409 by comparison between Figs. 4, 5 and 6. The higher the octane number, the



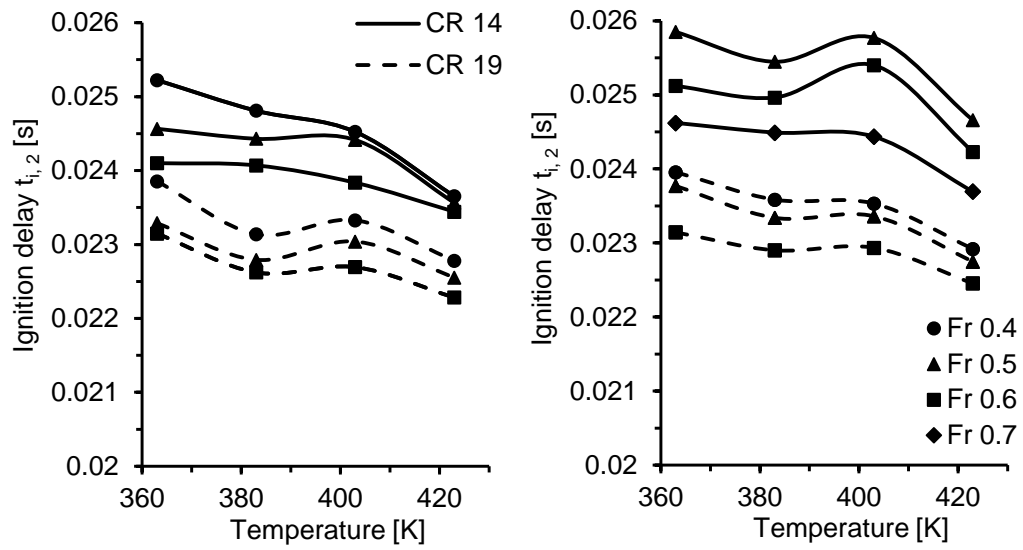


Figure 6: Ignition delay,  $t_{i,2}$ , versus initial temperature for PRF75. Both compression ratios are plotted. Left.-  $X_{O_2} = 0.21$ . Right.-  $X_{O_2} = 0.18$ .

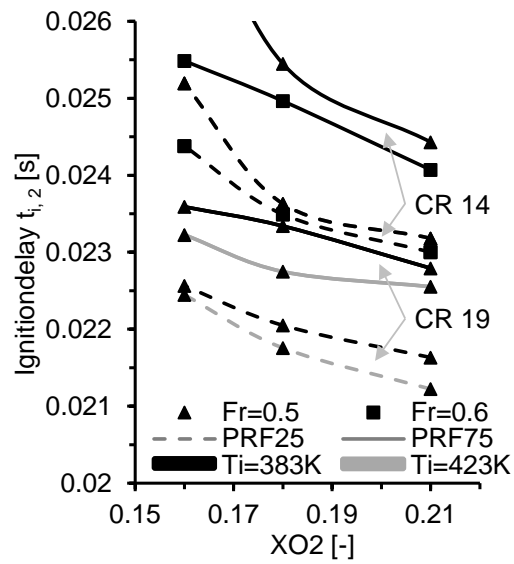


Figure 7: Ignition delay,  $t_{i,2}$ , versus molar fraction of oxygen for different fuels under different conditions. Triangular marks.- Fr = 0.5. Square marks.- Fr = 0.6. Dashed line.- PRF25. Solid line.- PRF75. Black line.-  $T_i = 383 K$ . Grey line.-  $T_i = 423 K$ . Both compression ratios are plotted.

410 longer the ignition delay, since the octane number represents, with strong  
411 non-linearity, the resistance of a certain fuel to autoignite. Differences in  
412 octane number are reflected in differences in cool flames intensity. Higher  
413 amounts of low-temperature heat release and higher quantities of  $\text{H}_2\text{O}_2$  are  
414 correlated with earlier ignition and lower octane values [38]. Furthermore,  
415 the fuel composition strongly affects the existence or not of a NTC behavior  
416 smooth enough to avoid a two-stage ignition pattern. In general, the higher  
417 the octane number the less prone is the fuel to show an NTC zone. Thus, the  
418 NTC behavior is a common phenomenon for alkanes. Finally, it should be  
419 noted that all fuels auto-ignite under low temperature conditions following  
420 chemical paths that include the NTC behavior. However, if the character-  
421 istic time (or relevance) of such phenomenon is short enough, it cannot be  
422 distinguish and a single-stage ignition pattern occurs.

423 According to cool flames, this phenomenon has shown to be highly de-  
424 pendent on temperature. The ignition delay referred to cool flames is always  
425 shorter if the temperature is increased. Obviously, cool flames are not af-  
426 fected by the loss of reactivity of the NTC behavior since it occurs before the  
427 NTC zone. Besides, the ignition delay referred to cool flames is also shorter  
428 if the compression ratio is increased, since higher temperatures and pressures  
429 are reached. Moreover, the ignition delay sensitivity to the equivalence ratio  
430 of the mixture is really low. On the one hand, the higher the equivalence  
431 ratio, the higher the reactivity of the mixture at low temperatures. However,  
432 on the other hand, the higher the equivalence ratio, the higher the heat capac-  
433 ity of the mixture and, therefore, the higher the thermal sink effect, leading  
434 to lower temperatures. The result of these two facts is that cool flames are

435 only slightly affected by the equivalence ratio. It should be mentioned that  
436 differences in heat capacity associated to different equivalence ratios are not  
437 important enough to see any effect on the ignition delay referred to the high  
438 exothermic stage. Finally, the ignition delay referred to cool flames is also  
439 shorter if the percent of oxygen is increased.

440 *3.2. Validation of the detailed chemical kinetic mechanism. Predictive meth-*  
441 *ods applied to cool flames*

442 Cool flames is only present in the cases performed with PRF25 and  
443 PRF50. The high octane number and the percentage of iso-octane of PRF75  
444 cause that cool flames cannot be clearly identified. As said before, two dif-  
445 ferent predictive methods have been tested. On the one hand, the integral  
446 method defined by Eq. 2 has been applied assuming HO<sub>2</sub> as chain carrier.  
447 On the other hand, the Livengood & Wu integral method (Eq. 1) has been  
448 solved using  $\tau_1$  values referred to cool flames.

449 The relative deviation in ignition delay,  $\epsilon$ , was calculated in order to more  
450 easily compare experimental and simulation results. This deviation is defined  
451 as follows:

$$\epsilon = \frac{t_{i,1x} - t_{i,1RCEM}}{t_{compression}} 100 \quad (4)$$

452 where  $t_{i,1}$  represents the ignition delay under transient conditions referred  
453 to cool flames. The subscript *RCEM* represents data obtained experimen-  
454 tally from the RCEM, whereas the subscript  $x$  can represent either results  
455 obtained from a chemical simulation with CHEMKIN using an IC-engine re-  
456 actor, *ICE*, from the alternative predictive method, *Int*, or from the Liven-

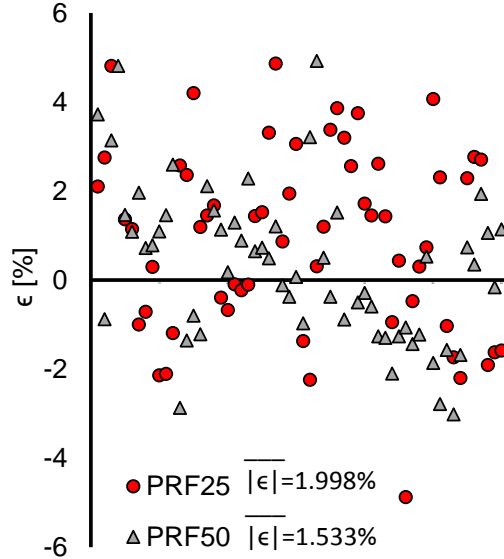


Figure 8: Percentage deviation in ignition delay referred to cool flames for PRF25 and PRF50. The mean absolute deviation,  $|\bar{\epsilon}|$ , shows good agreement between both experimental and simulated results.

457 good & Wu integral method,  $LW$ . It should be noted that the previous  
 458 definition for the deviation compares a difference between chemical times,  
 459  $t_{i,1x} - t_{i,1RCEM}$ , with the physical time of the process,  $t_{compression}$ . Therefore,  
 460  $\epsilon$  represents the difference of the inverse of the Damköhler number of both,  
 461 simulation and experiment ( $\epsilon = 1/Da_x - 1/Da_{RCEM}$ ).

462 The ignition delay deviations referred to cool flames between the chemical  
 463 kinetic simulations and the experimental results are shown in Fig. 8 for all  
 464 cases that show a two-stage ignition pattern. The mean absolute deviation,  
 465  $|\bar{\epsilon}|$ , has been also calculated.

466 The confidence intervals for the mean absolute deviation,  $|\bar{\epsilon}|$ , with a  
 467 confidence level of 95% are equal to  $[1.633, 2.362]$  % for PRF25 and to

468 [1.344, 1.984] % for PRF50, which means that the direct chemical simulations  
 469 performed with a detailed mechanism are able to replicate the experimen-  
 470 tal ignition delays. The predicted ignition delays also show to have quite  
 471 good accuracy. The confidence intervals for  $|\bar{\epsilon}|$  with a confidence level of  
 472 95% are summarized in Table 3 for the predictive methods. The values of  
 473  $|\bar{\epsilon}|$  are very similar to each other, meaning that both predictive methods are  
 474 able to predict the ignition delay referred to cool flames with approximately  
 475 the same accuracy than the detailed chemical kinetic mechanism. Therefore,  
 476 HO<sub>2</sub> seems to be a good tracer of cool flames. Furthermore, it should be  
 477 noted that the Livengood & Wu integral method can be used to predict cool  
 478 flames without having high deviations, even if a two-ignition pattern occurs.

	<b>PRF25</b>	<b>PRF50</b>
<b>ICE</b>	[1.633, 2.362]%	[1.344, 1.984]%
<b>New integral proposed</b>	[1.581, 2.238]%	[1.535, 2.351]%
<b>Livengood &amp; Wu</b>	[1.616, 2.227]%	[1.266, 2.001]%

Table 3: Confidence interval for the mean absolute deviation referred to cool flames,  $|\bar{\epsilon}|$ , with a confidence level of 95% for the chemical kinetic simulations (ICE) and for the different predictive methods.

479 Fig. 9 shows the ignition delay simulations and predictions versus the  
 480 experimental ignition delay referred to cool flames. The line  $y = x$  (per-  
 481 fect match between values), as well as the Pearson’s coefficient of correlation  
 482 ( $R^2$ ), has been also plotted in the figure. As it can be seen, numerical ig-  
 483 nition delays follow an aleatory distribution around the line  $y = x$ , which  
 484 means that ignition delay deviations are caused partly by the chemical ki-  
 485 netic mechanism used and partly by the experimental uncertainties mainly

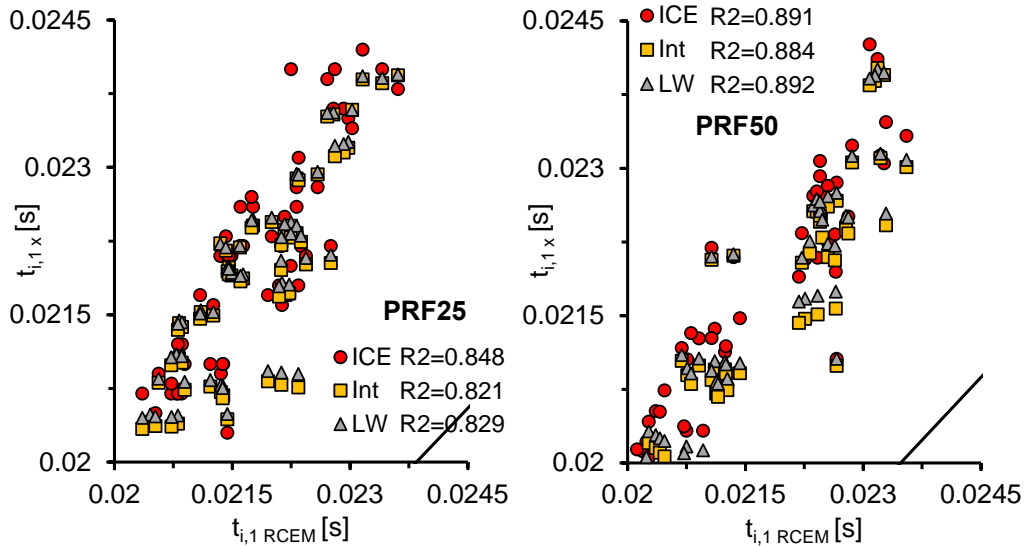


Figure 9: Ignition delay referred to cool flames,  $t_{i,1x}$ , from a chemical simulation with CHEMKIN using a closed 0-D IC-engine reactor,  $ICE$ , from the new predictive method,  $Int$ , and from the Livengood & Wu integral method,  $LW$ , versus the experimental ignition delay referred to cool flames,  $t_{i,1RCEM}$ . Left.- PRF25. Right.- PRF50.

486 associated to the calculation of the effective volume and the heat losses in  
 487 the RCEM.

488 *3.3. Validation of the detailed chemical kinetic mechanism. Predictive meth-*  
 489 *ods applied to the high exothermic stage*

490 Ignition delays referred to a maximum pressure rise rate are measured  
 491 experimentally in the RCEM and calculated by direct chemical kinetic sim-  
 492 ulations in CHEMKIN. The same two different predictive methods than the  
 493 ones used for cool flames have been evaluated. On the one hand, the alterna-  
 494 tive integral method proposed by Desantes et al. [20] (Eq. 2 and Eq. 3) has

495 been tested, assuming formaldehyde as chain carrier. On the other hand, the  
496 Livengood & Wu integral method (Eq. 1) has been solved by using  $\tau_2$  values  
497 referred to a maximum pressure rise.

498 The percentage deviation in ignition delay,  $\epsilon$ , was again calculated, the  
499 definition of which is analogous to the one used for cool flames (Eq. 4). Obvi-  
500 ously, in this case the relative deviation is calculated using the ignition delays  
501 under transient thermodynamic conditions referred to the high-temperature  
502 stage of the process.

503 The ignition delay deviations referred to the high-temperature stage be-  
504 tween the chemical kinetic simulations and the experimental results are  
505 shown in Fig. 10 for all cases. The mean absolute deviation,  $|\bar{\epsilon}|$ , has been  
506 calculated and its value can be seen in the figure.

507 The confidence interval for the mean absolute deviation,  $|\bar{\epsilon}|$ , with a confi-  
508 dence level of 95% is equal to [1.344, 1.984] % for PRF25, [1.809, 2.648] % for  
509 PRF50 and [2.463, 3.765] % for PRF75. It can be seen that the higher the  
510 octane number, the worse the simulation capability of the mechanism, which  
511 means that the accuracy of the n-heptane sub-mechanism is higher than the  
512 accuracy of the iso-octane sub-mechanism. The confidence intervals for  $|\bar{\epsilon}|$   
513 with a confidence level of 95% are summarized in Table 4 for all the predic-  
514 tive methods. The alternative predictive method tested in this paper shows  
515 to be quite accurate comparing to the experiments. However, the predictive  
516 capability of the Livengood & Wu integral method shows a strong depen-  
517 dence on the type of fuel. It can be seen that the Livengood & Wu integral is  
518 able to predict accurately the ignition delay referred to the high exothermic  
519 stage of combustion if the fuel shows a single-stage ignition (PRF75), but



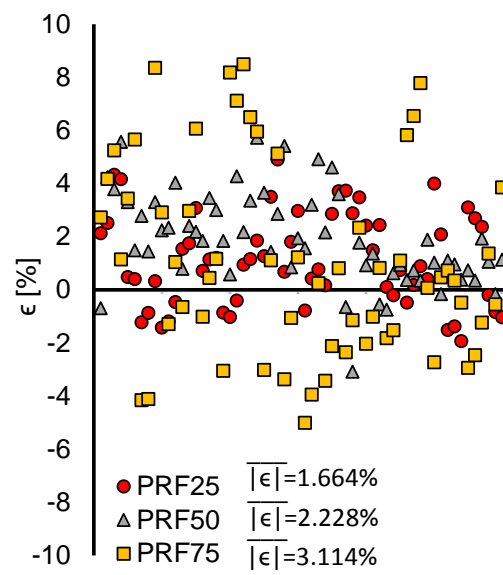


Figure 10: Percentage deviation in ignition delay referred to the high-temperature stage for all fuels. The mean absolute deviation,  $\overline{|\epsilon|}$ , shows a good agreement between both experimental and simulated results.

520 the predictive capability is significantly reduced when a two-stage ignition  
 521 occurs (PRF25 and PRF50).

	<b>PRF25</b>	<b>PRF50</b>	<b>PRF75</b>
<b>ICE</b>	[1.344, 1.984]%	[1.809, 2.648]%	[2.463, 3.765]%
<b>New integral proposed</b>	[2.061, 3.424]%	[2.635, 4.018]%	[1.740, 2.477]%
<b>Livengood &amp; Wu</b>	[4.603, 6.094]%	[6.513, 9.884]%	[1.901, 2.702]%

Table 4: Confidence interval for the mean absolute deviation referred to a maximum pressure rise,  $|\bar{\epsilon}|$ , with a confidence level of 95% for the chemical kinetic simulations (ICE) and for the different predictive methods.

522 Only ignition delays referred to a critical concentration of chain carriers  
 523 can be predicted by means of the Livengood & Wu integral method, since one  
 524 of its hypotheses is that autoignition occurs when a maximum concentration  
 525 of chain carriers is reached. In the same way, all the ignition characteristics  
 526 at constant conditions that are used in the integral ( $\tau$ ) have to be referred to  
 527 a critical concentration of chain carriers. Therefore, the predictions and the  
 528 ignition delays referred to the high-temperature stage are referred to different  
 529 stages of the ignition process, leading to a certain deviation. Obviously,  
 530 the smoother the NTC zone, the more similar the ignition delay referred  
 531 to a critical concentration and referred to a maximum pressure rise rate, so  
 532 that the accuracy of the Livengood & Wu integral is increased under these  
 533 conditions.

534 Fig. 11 shows the simulated and predicted ignition delay referred to the  
 535 high-temperature stage versus the experimental measurements. The line  
 536  $y = x$  (perfect match between values), as well as the Pearson's coefficient  
 537 of correlation ( $R^2$ ), has been also plotted in the figure. It can be seen that

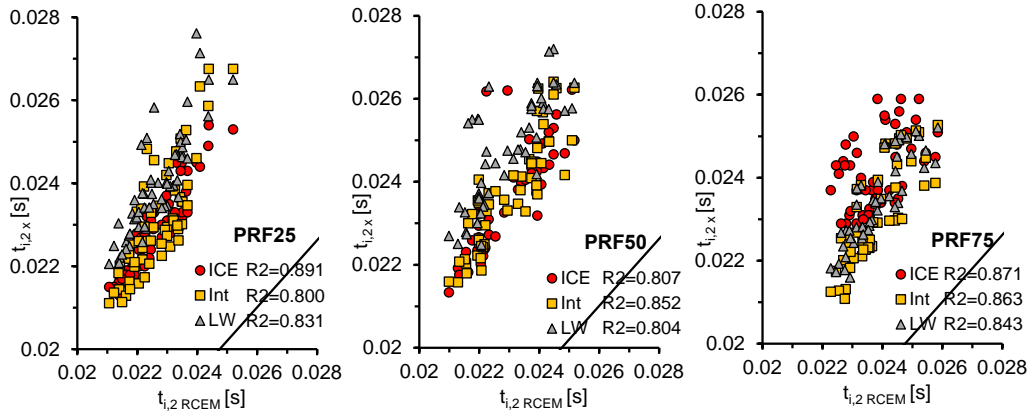


Figure 11: Ignition delay referred to the high temperature stage,  $t_{i,2,x}$ , from a chemical simulation with CHEMKIN using a closed 0-D IC-engine reactor, *ICE*, from the new predictive method, *Int*, and from the Livengood & Wu integral method, *LW*, versus the experimental ignition delay referred to the high temperature stage,  $t_{i,2,RCEM}$ . Left.- PRF25. Medium.- PRF50. Right.- PRF75.

538 the ignition delay referred to a maximum pressure rise is overestimated for  
 539 PRF25 and even more overestimated for PRF50. As explained in [22], this  
 540 fact can be caused by the isomerization rates of alkyl-peroxyl radicals and  
 541 peroxy-alkylhydroperoxyl radicals, which have been decreased by a factor of  
 542 three compared to n-heptane in the case of the iso-octane sub-mechanism.  
 543 Thus, higher percentage of iso-octane implies more overestimated ignition de-  
 544 lays. However, this trend cannot be seen for PRF75 because this phenomenon  
 545 is compensated by wall effects that are not present in the simulations. Thus,  
 546 the maximum pressure rise rate is reached much faster in the simulations  
 547 than in the experiments, which leads to a certain negative deviation between  
 548 models and experiments. The absence of wall effects and heterogeneities  
 549 in CHEMKIN causes a faster pressure rise, which leads to shorter ignition

550 delays and compensates the effect of the iso-octane sub-mechanism.

#### 551 **4. Conclusions**

552 In this work a detailed chemical kinetic mechanism has been validated for  
553 PRF mixtures versus experimental results obtained from a RCEM. Besides,  
554 the alternative method to predict ignition delays under transient conditions  
555 proposed by Desantes et al. [20] has been also validated by comparison to  
556 the experiments. Both ignition delays, the one referred to cool flames and  
557 the other one referred to a maximum pressure rise rate can be predicted  
558 with quite good accuracy. Finally, the predictive capability of the method  
559 has been compared to the Livengood & Wu integral, showing the alternative  
560 procedure better results than the classic Livengood & Wu method.

561 The following conclusions can be deduced from this study:

- 562 • Both predictive methods tested in this work can predict with quite good  
563 accuracy the ignition time referred to cool flames, demonstrating that  
564  $\text{HO}_2$  can be taken as a good cool flames tracer under a wide range of  
565 octane numbers and that the Livengood & Wu integral method works  
566 properly for cool flames.
  
- 567 • The alternative integral method has shown to be able to predict the  
568 ignition delays referred to a maximum pressure rise rate when  $\text{CH}_2\text{O}$   
569 is taken as chain carrier. This ignition delay can be experimentally  
570 measured, allowing a direct comparison between predictions and ex-  
571 periments.

572 • The high-temperature stage of the ignition can be predicted by means  
573 of the Livengood & Wu integral method only for fuels that do not  
574 show a two stage ignition pattern. I.e., in the present study the high  
575 exothermic stage can be predicted by this method only for PRF75,  
576 since the higher the octane number, the more prone is the fuel to show  
577 a single-stage ignition. These dependence on the type of fuel can be  
578 avoided by using the alternative integral method proposed by Desantes  
579 et al. [20].

580 **Acknowledgements**

581 The authors would like to thank different members of the CMT-Motores  
582 Térmicos team of the Universitat Politècnica de València for their contribu-  
583 tion to this work. The authors would also like to thank the Spanish Ministry  
584 of Education for financing the PhD. Studies of Darío López-Pintor (grant  
585 FPU13/02329). This work was partly founded by the Spanish Ministry of  
586 Economy and Competitiveness, project TRA2015-67136-R.

587 **Notation**

<i>BDC</i>	Bottom Dead Center
<i>CC</i>	Chain carriers
<i>CFD</i>	Computational Fluid Dynamics
<i>CI</i>	Compression Ignition
<i>CR</i>	Compression Ratio
<i>EGR</i>	Exhaust Gas Recirculation
<i>Fr</i>	Working equivalence ratio
588 <i>HCCI</i>	Homogeneous Charge Compression Ignition
<i>ICE</i>	Referred to data obtained from CHEMKIN using the internal combustion engine reactor
<i>Int</i>	Referred to data obtained from the new integral proposed in this paper
<i>LW</i>	Referred to data obtained from the Livengood & Wu integral method

<i>LTC</i>	Low Temperature Combustion
<i>max</i>	Referred to a maximum concentration of chain carriers
<i>NTC</i>	Negative Temperature Coefficient
$P_i$	Initial pressure
<i>PRF</i>	Primary Reference Fuels
<i>PSR</i>	Perfectly Stirred Reactor
<i>RCEM</i>	Rapid Compression-Expansion Machine
<i>SI</i>	Spark Ignition
$T_i$	Initial temperature
<i>TDC</i>	Top Dead Center
$t_i$	Ignition delay under transient conditions
$t_{i,CC}$	Ignition delay referred to the critical concentration of chain carriers
$t_{i,1}$	Ignition delay referred to the maximum pressure rise of cool flames
$t_{i,2}$	Ignition delay referred to the maximum pressure rise
<i>UHC</i>	Unburned hydrocarbons
$X_{O_2}$	Oxygen molar fraction
$\epsilon$	Percentage deviation in ignition delay between experimental and simulation or predicted results
$ \bar{\epsilon} $	Mean absolute deviation between experimental and simulation or predicted results
$\tau$	Ignition delay under constant conditions of pressure and temperature

$\tau_{CC}$	Ignition delay under constant thermodynamic conditions referred to the critical concentration of chain carriers
$\tau_1$	Ignition delay under constant thermodynamic conditions referred to the maximum pressure rise of cool flames
$\tau_2$	Ignition delay under constant thermodynamic conditions referred to the maximum pressure rise

## References

- [1] J. Benajes, S. Molina, A. García, and J. Monsalve-Serrano. Effects of direct injection timing and blending ratio on RCCI combustion with different low reactivity fuels. *Energy Conversion and Management*, 99:193–209, 2015.
- [2] Z. Zheng, L. Yue, H. Liu, Y. Zhu, X. Zhong, and M-Yao. Effect of two-stage injection on combustion and emissions under high EGR rate on a diesel engine by fueling blends of diesel/gasoline, diesel/n-butanol, diesel/gasoline/n-butanol and pure diesel. *Energy Conversion and Management*, 90:1–11, 2015.
- [3] T. Li, D. Wu, and M. Xu. Thermodynamic analysis of EGR effects on the first and second law efficiencies of a boosted spark-ignited direct-injection gasoline engine. *Energy Conversion and Management*, 70:130–138, 2013.
- [4] S.S. Nathan, J.M. Mallikarjuna, and A. Ramesh. An experimental study



- 606 of the biogas-diesel HCCI mode of engine operation. *Energy Conversion*  
607 *and Management*, 51:1347–1353, 2010.
- 608 [5] J. Benajes, J.V. Pastor, A. García, and J. Monsalve-Serrano. An exper-  
609 imental investigation on the influence of piston bowl geometry on RCCI  
610 performance and emissions in a heavy-duty engine. *Energy Conversion*  
611 *and Management*, 103:1019–1030, 2015.
- 612 [6] K. Bahlouli, U. Atikol, R.K. Saray, and V. Mohammadi. A reduced  
613 mechanism for predicting the ignition timing of a fuel blend of natural-  
614 gas and n-heptane in HCCI engine. *Energy Conversion and Manage-*  
615 *ment*, 79:85–96, 2014.
- 616 [7] J.C. Livengood and P.C. Wu. Correlation of autoignition phenomena in  
617 internal combustion engines and rapid compression machines. *Sympo-*  
618 *sium (International) on Combustion*, 5:347–356, 1955.
- 619 [8] L. Chen, T. Li, T. Yin, and B. Zheng. A predictive model for knock  
620 onset in spark-ignition engines with cooled EGR. *Energy Conversion*  
621 *and Management*, 87:946–955, 2014.
- 622 [9] M. Shahbakhti, R. Lupul, and C. R. Koch. Predicting HCCI auto-  
623 ignition timing by extending a modified knock-integral method. *SAE*  
624 *Paper no. 2007-01-0222*, 2007.
- 625 [10] Y. Ohyama. Engine control using a combustion model. *Seoul 2000*  
626 *FISITA World Automotive Congress*, 2000.
- 627 [11] D.J. Rausen, A.G. Stefanopoulou, J.M. Kang, J.A. Eng, and T.W. Kuo.  
628 A mean-value model for control of homogeneous charge compression

- 629 ignition HCCI engines. *Journal of Dynamic Systems, Measurement,*  
630 *and Control*, 127:355–362, 2005.
- 631 [12] Y. Choi and J.Y. Chen. Fast prediction of start-of-combustion in HCCI  
632 with combined artificial neural networks and ignition delay model. *Pro-*  
633 *ceedings of the Combustion Institute*, 30:2711–2718, 2005.
- 634 [13] M. Hillion, J. Chauvin, and N. Petit. Control of highly diluted com-  
635 bustion in diesel engines. *Control Engineering Practice*, 19:1274–1286,  
636 2011.
- 637 [14] A.D.B. Yates, A. Swarts, and C.L. Viljoen. Correlating auto-ignition  
638 delays and knock-limited spark-advance data for different types of fuel.  
639 *SAE Paper no. 2005-01-2083*, 2005.
- 640 [15] L. Liang and R.D. Reitz. Spark ignition engine combustion modeling  
641 using a level set method with detailed chemistry. *SAE Paper no. 2006-*  
642 *01-0243*, 2006.
- 643 [16] R. Edenhofer, K. Lucka, and H. Kohne. Low temperature oxidation of  
644 diesel-air mixtures at atmospheric pressure. *Proceedings of the Combustion*  
645 *Institute*, 31:2947–2954, 2007.
- 646 [17] J.J. Hernandez, M. Lapuerta, and J. Sanz-Argent. Autoignition pre-  
647 diction capability of the Livengood-Wu correlation applied to fuels of  
648 commercial interest. *International Journal of Engine Research*, 15:817–  
649 829, 2014.
- 650 [18] J. M. Desantes, J. J. López, S. Molina, and D. López-Pintor. Validity  
651 of the Livengood & Wu correlation and theoretical development of an

- 652 alternative procedure to predict ignition delays under variable thermo-  
653 dynamic conditions. *Energy Conversion and Management*, 105:836–847,  
654 2015.
- 655 [19] J. M. Desantes, J. J. López, S. Molina, and D. López-Pintor. Theo-  
656 retical development of a new procedure to predict ignition delays un-  
657 der transient thermodynamic conditions and validation using a Rapid  
658 Compression-Expansion Machine. *Energy Conversion and Management*,  
659 108:132–143, 2016.
- 660 [20] J. M. Desantes, , V. Bermúdez, J. J. López, and D. López-Pintor. A  
661 new method to predict high and low-temperature ignition delays under  
662 transient thermodynamic conditions and its experimental validation us-  
663 ing a Rapid Compression-Expansion Machine. *Energy Conversion and*  
664 *Management*, 123:512–522, 2016.
- 665 [21] P.W. Bessonette, C.H. Schleyer, K.P. Duffy, W.L. Hardy, and M.P.  
666 Liechty. Effects of fuel property changes on heavy-duty HCCI com-  
667 bustion. *SAE Paper no. 2007-01-0191*, 2007.
- 668 [22] J. M. Desantes, J.M. García-Oliver, W. Vera-Tudela, D. López-Pintor,  
669 B. Schneider, and K. Boulouchos. Study of ignition delay time and  
670 generalization of auto-ignition for PRFs in a RCEM by means of natural  
671 chemiluminescence. *Energy Conversion and Management*, 111:217–228,  
672 2016.
- 673 [23] G. Barroso, A. Escher, and K. Boulouchos. Experimental and numerical  
674 investigations on HCCI combustion. *SAE Paper no. 2005-24-038*, 2005.

- 675 [24] S. Schlatter, B. Schneider, Y. Wright, and K. Boulouchos. Compara-  
676 tive study of ignition systems for lean burn gas engines in an optically  
677 accessible Rapid Compression Expansion Machine. *SAE Paper no. 2013-*  
678 *24-0112*, 2013.
- 679 [25] T. Steinhilber and T. Sattelmayer. The effect of water addition on HCCI  
680 diesel combustion. *SAE Paper no. 2006-01-3321*, 2006.
- 681 [26] R. Payri, F.J. Salvador, J. Gimeno, and G. Bracho. A new methodol-  
682 ogy for correcting the signal cumulative phenomenon on injection rate  
683 measurements. *Experimental Techniques*, 32:46–49, 2008.
- 684 [27] J. M. Desantes, J. J. López, S. Molina, and D. López-Pintor. Design  
685 of synthetic EGR and simulation study of the effect of simplified for-  
686 mulations on the ignition delay of isooctane and n-heptane. *Energy*  
687 *Conversion and Management*, 96:521–531, 2015.
- 688 [28] J. Benajes, P. Olmeda, J. Martín, and R. Carreño. A new methodology  
689 for uncertainties characterization in combustion diagnosis and thermo-  
690 dynamic modelling. *Applied Thermal Engineering*, 71:389–399, 2014.
- 691 [29] F. Payri, S. Molina, J. Martín, and O. Armas. Influence of measure-  
692 ment errors and estimated parameters on combustion diagnosis. *Applied*  
693 *Thermal Engineering*, 26:226–236, 2006.
- 694 [30] G. Woschni. A universally applicable equation for the instantaneous  
695 heat transfer coefficient in the internal combustion engine. *SAE Paper*  
696 *no. 670931*, 1967.

- 697 [31] B. Baeuerle, J. Warnatz, , and F. Behrendt. Time-resolved investigation  
698 of hot spots in the end gas of an S.I. engine by means of 2-D double-  
699 pulse LIF of formaldehyde. *Symposium (International) on Combustion*,  
700 2:2619–2626, 1996.
- 701 [32] H.J. Curran, P. Gaffuri, Pitz W.J, and C.K. Westbrook. A comprehen-  
702 sive modeling study of n-heptane oxidation. *Combustion and Flame*,  
703 114:149–177, 1998.
- 704 [33] H.J. Curran, P. Gaffuri, Pitz W.J, and C.K. Westbrook. A comprehen-  
705 sive modeling study of iso-octane oxidation. *Combustion and Flame*,  
706 129:253–280, 2002.
- 707 [34] M. Sjoberg and J.E. Dec. An investigation into lowest acceptable com-  
708 bustion temperatures for hydrocarbon fuel in HCCI engines. *Proceedings*  
709 *of the Combustion Institute*, 30:2719–2726, 2005.
- 710 [35] H.J. Curran, W.J. Pitz, C.K. Westbrook, C.V. Callahan, and F.L. Dryer.  
711 Oxidation of automotive primary reference fuels at elevated pressures.  
712 *Proceedings of the Combustion Institute*, 27:379–387, 1998.
- 713 [36] F. Payri, X. Margot, S. Patouna, F. Ravet, and M. Funk. Use of a  
714 single-zone thermodynamic model with detailed chemistry to study a  
715 natural gas fueled Homogeneous Charge Compression Ignition engine.  
716 *Energy Conversion and Management*, 53:298–304, 2012.
- 717 [37] I. Glassman and R.A. Yetter. *Combustion*. Elsevier Academic Press,  
718 2008.

719 [38] N. Blin-Simiand, R. Rigny, V. Viossat, S. Circan, and K. Sahetchian.  
720 Autoignition of hydrocarbon/air mixtures in a CFR engine: Experi-  
721 mental and modeling study. *Combustion Science and Technology*, 88(5-  
722 6):329–348, 1993.